Counting Classical Nodes in Quantum Networks

He Lu[1,2,3],* Chien-Ying Huang[4],* Zheng-Da Li[1,2], Xu-Fei Yin[1,2], Rui Zhang[1,2],
Teh-Lu Liao[4], Yu-Ao Chen[1,2],† Che-Ming Li[4,5,6],‡ and Jian-Wei Pan[1,2]§

[1]*Shanghai Branch, National Laboratory for Physical Sciences at Microscale and Department of Modern Physics,
University of Science and Technology of China, Shanghai 201315, China*
[2]*Synergetic Innovation Center of Quantum Information and Quantum Physics,
University of Science and Technology of China, Hefei, Anhui 230026, China*
[3]*School of Physics, Shandong University, Jinan 250100, China*
[4]*Department of Engineering Science, National Cheng Kung University, Tainan 701, Taiwan*
[5]*Center for Quantum Frontiers of Research & Technology,
National Cheng Kung University, Tainan, 701, Taiwan and*
[6]*Center for Quantum Technology, Hsinchu, 30013, Taiwan*
(Dated: July 19, 2022)

Quantum networks illustrate the use of connected nodes of quantum systems as the backbone of distributed quantum information processing. When the network nodes are entangled in graph states, such quantum platform is indispensable to almost all the existing distributed quantum tasks. Unfortunately, real networks unavoidably suffer from noise and technical restrictions, making nodes transit from quantum to classical at worst. Here, we introduce a figure of merit in terms of the number of classical nodes for quantum networks in arbitrary graph states. Such network property is revealed by exploiting a novel Einstein-Podolsky-Rosen steerability. Experimentally, we demonstrate photonic quantum networks of n_q quantum nodes and n_c classical nodes with n_q up to 6 and n_c up to 18 using spontaneous parametric down-conversion entanglement sources. We show that the proposed method is faithful in quantifying the classical defects in prepared multiphoton quantum networks. Our results provide novel identification of generic quantum networks and non-classical correlations in graph states.

Quantum mechanics enables non-classical correlations to exist across the whole of network via connecting individual quantum nodes, forming a joint quantum many-body system [1]. Quantum networks [2, 3] have far greater capacity than the classical ones and serve as well-advanced transmitters of quantum information for all the distant network participants. Such utilities encourage important applications in distributed quantum information processing, from quantum secret sharing (QSS) [4–9] to distributed sensing [10, 11], from distributed quantum computation [12–15] to quantum conference key agreement and distribution [16–18]. The physical realization of these distributed quantum tasks requires suitable connectivities between nodes and network topologies to initialize the nodes in the multipartite entangled states, known as *graph states* [19] (see Fig. 1a).

To establish a quantum network in graph states with tailored topology, quantum information demands to be sent, received, stored and exchanged between remote quantum nodes via photonic channels in general [1–3, 20–29]. Then, it is essential to characterize a created network before it carries out a given distributed task, such as QSS scheme. A conventional way to detect entanglement in laboratory is entanglement witness (EW), which employs deduction from the predictions of quantum theory [30–32]. However, inevitable imperfections of network nodes, such as the intrinsic fragility of quantum systems and errors present in actual implementations, can cause quantum nodes to become classical systems that obey the laws of classical physics, therefore leading to the fail-

ure of state preparation or decay of quantum networks [1–3, 20–29]. Moreover, when network participants only have limited knowledge about the node imperfections, the network nodes then become untrusted to the participants as untrusted nodes. Considering the existence of untrusted nodes in the created network, EW is no longer reliable in verification of multipartite entanglement. This raises a natural question: How a verifier, such as the dealer in QSS, objectively and reliably detect the presence of classical nodes in a given network for distributed tasks?

In this Letter, we address this issue by exploiting a novel Einstein-Podolsky-Rosen (EPR) steerability [33–35], which is capable of excluding the existing of classical nodes in quantum networks. More importantly, the EPR steerability presents more fine-grained information about the created network, i.e., the capability of counting the number of classical nodes in the created network, which is not possible in other schemes [32, 36].

Given an ideal N-node quantum network in arbitrary graph state $|G\rangle$, where each node contains a qubit, its general state decomposition can be explicitly expressed as [38, 39]

$$|G\rangle\langle G| = \sum_{\vec{m}} h_{\vec{m}} \bigotimes_{k=1}^{N} \hat{R}_{m_k}, \qquad (1)$$

where $h_{\vec{m}}$ are coefficients and $\hat{R}_{m_k}$ represents the m_kth observable of the kth node. We then introduce the network fidelity function for arbitrary target graph states
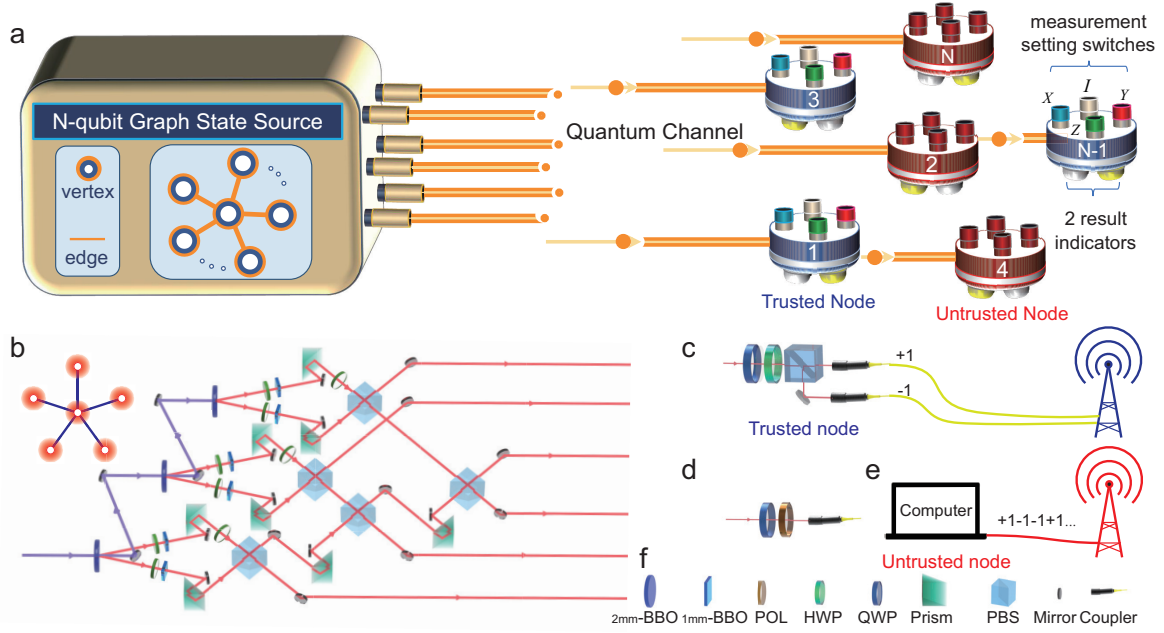
FIG. 1. Schematic drawing of the quantum network in graph state and its experimental realization. (a) a quantum network ideally prepared in a graph state is depicted using a graph $G(V, E)$ [19, 37]. The graph G consists of the vertex set V and the set E of edges each of which joins two vertices. The vertices and the edges physically represent the qubits and the interacting pairs of qubits respectively, and then constitute a state vector $|G\rangle$ of the network. A quantum network in graph state $|G\rangle$ is then distributed to distant nodes and verified by measurement apparatus. The measurement setting is chosen from set $\{I, X, Y, Z\}$, each of which has two outcomes $+1$ and -1. The blue (red) measurement apparatus represents trusted (untrusted) nodes in quantum network. It has been shown that arbitrary graph states among the network participants for distributed tasks can be established through a modular and plug-and-play architecture [25]. (b) the experimental setup to generate a six-photon state in star graph, which is equivalent to $|GHZ\rangle_6$ via LOCC. (c) the experimental setup to measure network fidelity F. (d) the experimental setup to generate the state in the optimal "cheating strategy", in which we project one photon on $|\xi'\rangle$ according to the target state $|G\rangle$. (e) the untrusted node broadcasts results according to measurement setting of $F(6)$ (see Supplementary Material for details [37]). (f) Symbols used in (b), (c) and (d): 2mm-long BBO crystal (2mm-BBO), 1mm-long BBO crystal (1-mm BBO), polarizer (POL), half-wave plate (HWP), quarter-wave plate (QWP) and polarization beam splitter (PBS).

$|G\rangle$ of N nodes

$$F(N) = \sum_{\vec{m}} h_{\vec{m}} \langle R_{m_1}...R_{m_N} \rangle \qquad (2)$$

where $\vec{m} \equiv (m_1, ..., m_N)$ and R_{m_k} is the outcome of the m_kth measurement of $\hat{R}_{m_k}$ on the kth node. In our study, the measurements on each qubit are performed with the observables in Pauli matrices, $\{\hat{R}_{m_k}|m_k = 0, 1, 2, 3\}$, where $\hat{R}_0 = I$, $\hat{R}_1 = X$, $\hat{R}_2 = Y$, and $\hat{R}_3 = Z$. Note that the fidelity function (2) is state-dependent and we obtain $F = 1$ for an ideal quantum network regardless of what fidelity function is chosen. We utilize the network fidelity function, which measures the closeness of created networks and target graph states, as the basis for counting classical nodes. This makes our framework capable of being used in a wide variety of circumstances and applications based on the fidelity measure.

When classical nodes exist in the created network, the network becomes a hybrid system consisting of n_q quantum nodes and n_c classical nodes, where $N = n_q + n_c$. The index set of the network nodes, V, can then be divided into the quantum-node subset, V_Q, and the classical-node subset, V_c, accordingly. An essential difference between quantum and classical nodes is that physical properties of quantum nodes might not have definite values. In contrast, variables in classical nodes are in existing states independent of observation, known as the assumption of *realism* [40–42]. In our framework, a node is defined as being *classical* if, for any physical properties of interest, it is classical realistic, i.e., the state of each classical node can be specified by a pre-existing and fixed set of measurement outcomes [35]. Note that with the increase of noises, the quantum nodes can eventually be described by the classical realistic theory. See Supplementary Material (SM) for detailed discussion of classical nodes [37].

Before the state decays, the state vector of the target graph state can always be represented in the Schmidt form of rank r [43]

$$|G\rangle = \frac{1}{\sqrt{r}} \sum_{v=0}^{r-1} |v\rangle_{sQ} |v\rangle_{sc}, \qquad (3)$$
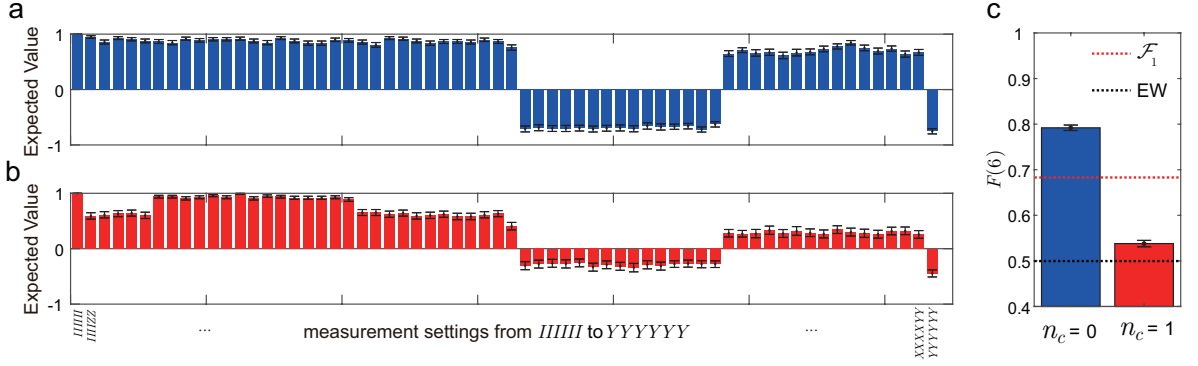
FIG. 2. Experimental results of network fidelity $F(6)$ of six-node network with classical node number $n_c = 0$ and $n_c = 1$ respectively. (a) the experimental results of network fidelity in network with $n_c = 0$. (b) the experimental results of network fidelity measurement in network with $n_c = 1$. (c) the calculated $F(6)$ from the results in (a) and (b). The black dash line is the threshold of EW, and the red dash line is the threshold fidelity $\mathcal{F}_1$.

for $r \geq 2$, where $\{|v\rangle_{sQ}\}$ and $\{|v\rangle_{sc}\}$ are the Schmidt bases for the nodes in the vertex sets V_Q and V_c, respectively. This representation shows us the following form under the state decomposition (8) for the nodes in V_c

$$|G\rangle\langle G| = \frac{1}{r} \sum_{v,v',\vec{m}_c} h_{\vec{m}_c}^{vv'} |v\rangle_{sQsQ}\langle v'| \bigotimes_{k \in V_c} \hat{R}_{m_k}, \quad (4)$$

where $|v\rangle_{scsc}\langle v'| = \sum_{\vec{m}_c} h_{\vec{m}_c}^{vv'} \bigotimes_{k \in V_c} \hat{R}_{m_k}$, $\vec{m}_c \equiv \{m_k | k \in V_c\}$, and $h_{\vec{m}_c}^{vv'}$ denote the decomposition coefficients. With the classical realistic theory to give a complete description of the total state of the n_c classical nodes in terms of the pre-existing outcome sets: $\{\mathbf{v}_k | k \in V_c\}$, the network fidelity function (2) can be rephrased as the following explicit form

$$F = \frac{1}{r} \sum_{v,v',\vec{m}_c} h_{\vec{m}_c}^{vv'} \left\langle |v\rangle_{sQsQ}\langle v'| \right\rangle \left\langle \prod_{k \in V_c} R_{m_k} \right\rangle. \quad (5)$$

The maximum fidelities between target graph states $|G\rangle$ and N-node networks having n_c classical nodes can then be described by the equation

$$\mathcal{F}_{n_c} = \frac{1}{4}(1 + 2^{\frac{-n_c}{2}} \sqrt{4 + 2^{n_c}}), \quad (6)$$

where $1 \leq n_c \leq N - 1$, holding for arbitrary target graph states (See SM for the detailed derivation [37]). The threshold fidelities $\mathcal{F}_{n_c}$ are strictly decreasing with the number of classical nodes n_c. It turns out that there exists a one-to-one correspondence between the number of classical nodes and the relevant maximum fidelity values. For instance, $\mathcal{F}_1 \simeq 0.6830$, $\mathcal{F}_2 \simeq 0.6036$, and $\lim_{n_c \to \infty} \mathcal{F}_{n_c} \simeq 0.5000$. The hybrids of quantum and classical nodes are then comparable in fidelity to the netwroks composed entirely of quantum nodes with $F \leq \mathcal{F}_1$. This implies that the collection $\{\mathcal{F}_{n_c}\} \equiv \{\mathcal{F}_{n_c} | n_c = 1, 2, ..., N - 1\}$ of the threshold fidelities can serve as a set of graduations to indicate the

degree of network imperfection. That is, if the measured fidelity F is found to be $\mathcal{F}_{n'_c+1} < F \leq \mathcal{F}_{n'_c}$, then one can infer that there are n'_c classical nodes in the created network. Note that the pre-existing state model used here is distinct from hidden variable models, such as the Mermin-Peres square, where noncontextual outcomes apply to each of nine observables for the tests of state-independent quantum contextuality in two-qubit systems [40, 44–48]. By contrast, our quantum-classical hybrid model for the derivation of $\mathcal{F}_{n_c}$ combines both pre-existing outcomes from n_c classical nodes and quantum measurements performed in n_q quantum nodes.

Indeed, the collection $\{\mathcal{F}_{n_c}\}$ quantitatively describes how the non-classical correlations among nodes of the graph states vary between the quantum-classical hybrids. If $F > \mathcal{F}_{n_c}$ for a created network, then it is impossible to simulate the correlations between nodes using any networks mixed with classical defects of the minimum classical nodes, n_c. Such a quantum characteristic can be interpreted as the genuine multi-subsystem EPR steering [37], a new type of genuine multipartite EPR steerability [49] of graph states [35]. Notably, the new-found criterion $F > \mathcal{F}_{n_c}$ is stricter than EW $F > 1/2$ for genuine multipartite entanglement [30–32] of networks, in which a network containing classical nodes can mimic the networks with genuine multipartite entanglement to show $1/2 < F < \mathcal{F}_1$. This serious flaw makes EW unreliable in verification of genuine multipartite entanglement for distributed quantum tasks.

We experimentally demonstrate our protocol on multipartite graph states in star graph $|G_N^{star}\rangle$, which is equivalent to Greenberg-Horne-Zeilinger (GHZ) state $|GHZ\rangle_N = \frac{1}{\sqrt{2}}(|0\rangle^{\otimes N} + |1\rangle^{\otimes N})$ via local operation and classical communication (LOCC). The experimental setup to generate a six-photon GHZ state $|GHZ\rangle_6 = \frac{1}{\sqrt{2}}(|H\rangle^{\otimes 6} + |V\rangle^{\otimes 6})$ with H the horizontal polarization and V the vertical polarization is shown in Fig. 1b.
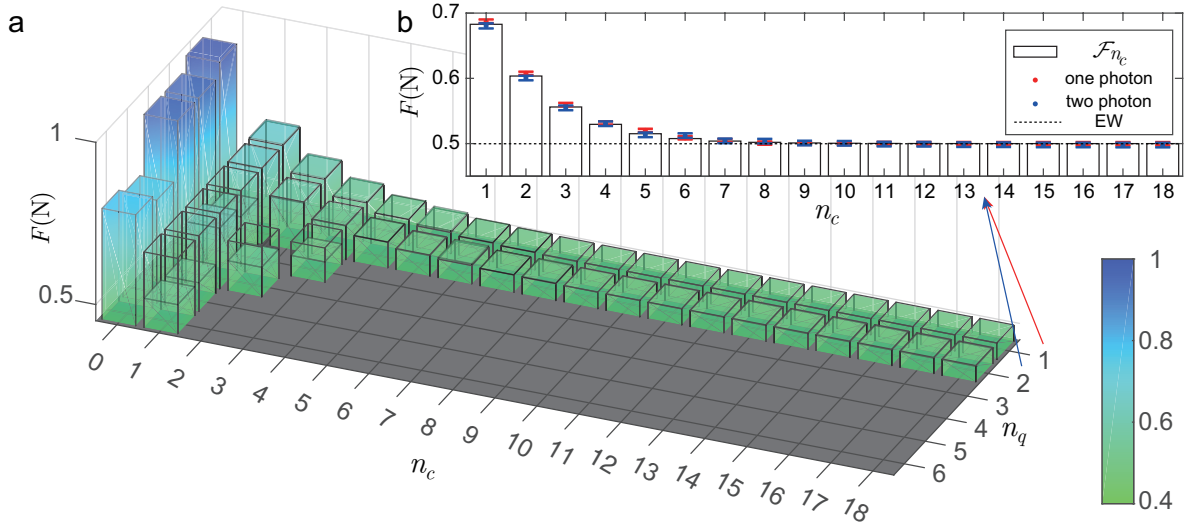
FIG. 3. Experimental results of network fidelity $F(N)$ in network with variant quantum and classical node number n_q and n_c, respectively. (a) the bars edged with black line represent threshold of network fidelity $\mathcal{F}_{n_c}$. The filled color bars represent the experimental measured network fidelity $F(N)$ in its corresponding network. (b) the results of $F(N)$ in networks with $n_q = 1$ and $n_q = 2$. The bars represent $\mathcal{F}_{n_c}$, and red (blue) dots represent the measured $F(N)$ in the network with $n_q = 1$ ($n_q = 2$).

An experimental state, denoted as ρ_6^{GHZ}, is generated by employing the typical spontaneous parametric down-conversion entangled photon source and photonic interferometry technologies (see SM for more details [37]). The network fidelity $F(6)$ of the generated state ρ_6^{GHZ} is measured by the device shown in Fig. 1c, which is consisted of a quarter-wave plate (QWP), half-wave plate (HWP), a polarization beam splitter (PBS) and two detectors. By properly choosing the angle of QWP and HWP, the expected value of I, X, Y and Z can be readout. The experimental results of measured $F(6)$ are shown in Fig. 2a, from which we calculate that $F(6) = 0.792 \pm 0.006$ (shown with blue bar in Fig. 2c). Then $F(6)$ exceeds the threshold fidelity $\mathcal{F}_1 = 0.683$ more than 18 standard deviation, which indicates there is no classical node in the tested network.

We then consider the case where n_c classical nodes exist in the N-node network, and show that $F(N)$ is bounded by the threshold fidelity $\mathcal{F}_{n_c}$ even with the optimal "cheating strategy" (OCS). The OCS of one untrusted node in bipartite quantum correlation has been well discussed [50]. We generalize the OCS of n_c untrusted (classical) nodes with a lack of N-partite entanglement to cheat the other trusted participants in the N-node network as: the n_c untrusted nodes first prepare the entangled state $|\xi\rangle_{n_q}$ for n_q trusted (quantum) nodes based on their knowledge of the N-node network, where $n_q = N - n_c$. Then, according to the measurement setting for the network fidelity function (2), the n_c untrusted nodes broadcast their results $\in \{+1, -1\}$ to achieve the maximal $F(N)$ [37]. The experimental results of $F(6)$ under the OCS are shown in Fig. 2b, from which we calculate $F(6) = 0.538 \pm 0.007$ (shown with red bar in

Fig. 2c). As shown in Fig. 3a, we can see that $F(6)$ either with $n_c = 0$ or $n_c = 1$ exceeds the EW threshold [32], which is a strong evidence that EW is no longer reliable in quantum network identification. However, with our criteria, the measured $F(6)$ does not exceed the threshold fidelity $\mathcal{F}_1$, which indicates there are classical nodes in the measured network. One may notice that, in the case of $n_c = 1$ under the OCS, $F(6) = 0.538 \pm 0.007$ is lower than $\mathcal{F}_3$ but higher than $\mathcal{F}_4$, where the fidelity threshold overcounts the number of classical nodes in the created network. This is caused by the imperfections in the state preparation, where $F(6) = 0.792 \pm 0.006$ in the case of $n_c = 0$, and such imperfections prevents us from achieving the optimal fidelity $\mathcal{F}_1 \simeq 0.6830$ with the OCS. These imperfections can be evaluated by our fidelity criteria in terms of the number of classical nodes. For $\mathcal{F}_4 < F(6) = 0.538 \pm 0.007 < \mathcal{F}_3$, the quantity of classical defects in the created network effectively equals to three classical nodes with the optimal mimicry.

We also experimentally prepare various N-node quantum networks with n_q up to 6 and n_c up to 18, where $N = n_q + n_c$ [37]. For each network, n_c nodes employ OCS to achieve maximal network fidelity $F(N)$. The measured $F(N)$ are shown in Fig. 3a. It is clear that $F(N)$ with n_c classical nodes are bounded by the threshold fidelity $\mathcal{F}_{n_c}$. One may notice that $F(N)$ decreases much faster than $\mathcal{F}_{n_c}$ as n_q increased. This is mainly caused by the imperfections in the state preparation, in which more imperfections are introduced when coherently manipulating more photons. When $n_q \geq 3$, $F(N)$ decreases below EW threshold (0.5) quickly as n_c increased ($n_c \geq 4$). We investigate $F(N)$ of networks with $n_q = 1$ and $n_q = 2$ for large n_c as the prepared

one-photon and two-photon states are with near unity fidelities. The results of $F(N)$ for $n_q = 1$ and $n_q = 2$ are particularly shown in Fig. 3b, from which we can see that $F(N)$ fits $\mathcal{F}_{n_c}$ very well. We analyze the standard deviation $\mathcal{E}$ of $F(N)$ in verifying entanglement and evaluating n_c. We observe $\mathcal{E} > 3$ when $n_c \leq 6$ in the created network with $n_q = 1$ and $n_q = 2$, which reflects a high confidence level of our criteria (See Supplementary Material for more experimental details).

Our findings, to the best of our knowledge, is the first method capable of counting the number of classical nodes in quantum networks. Moreover, the proposed method reveals that the quantum-classical hybrid networks with OCS can surpass the seminal EW threshold of $F > 1/2$, which causes serious flaws in using the verification of EW in quantum networks [32]. Our proof-of-principle photonic networking experiments, with n_q up to 6 and n_c up to 18, validated the proposed threshold network fidelities $\mathcal{F}_{n_c}$, and showed the failure of using EW for genuine multipartite entanglement verification. Our results therefore not only open a new way to characterize classical defects in quantum networks [1–3, 20–29] for a wide range of distributed quantum tasks [4–18], but also provide novel insights in multipartite non-classical correlations in graph states [51–53]. We expect that our formalism could be extended to the other types of quantum states, such as W states, for characterization of multipartite entanglement with further studies [30, 31, 54].

---

* These two authors contributed equally to this work
† yuaochen@ustc.edu.cn
‡ cmli@mail.ncku.edu.tw
§ pan@ustc.edu.cn

[1] S. Ritter, C. Nölleke, C. Hahn, A. Reiserer, A. Neuzner, M. Uphoff, M. Mücke, E. Figueroa, J. Bochmann, and G. Rempe, Nature **484**, 195 (2012).
[2] H. J. Kimble, Nature **453**, 1023 (2008).
[3] S. Wehner, D. Elkouss, and R. Hanson, Science **362**, eaam9288 (2018).
[4] M. Hillery, V. Bužek, and A. Berthiaume, Phys. Rev. A **59**, 1829 (1999).
[5] Y.-A. Chen, A.-N. Zhang, Z. Zhao, X.-Q. Zhou, C.-Y. Lu, C.-Z. Peng, T. Yang, and J.-W. Pan, Phys. Rev. Lett. **95**, 200502 (2005).
[6] D. Markham and B. C. Sanders, Phys. Rev. A **78**, 042309 (2008).
[7] B. A. Bell, D. Markham, D. A. Herrera-Martí, A. Marin, W. J. Wadsworth, J. G. Rarity, and M. S. Tame, Nat. Commun. **5**, 5480 EP (2014).
[8] H. Lu, Z. Zhang, L.-K. Chen, Z.-D. Li, C. Liu, L. Li, N.-L. Liu, X. Ma, Y.-A. Chen, and J.-W. Pan, Phys. Rev. Lett. **117**, 030501 (2016).
[9] C.-Y. Huang, N. Lambert, C.-M. Li, Y.-T. Lu, and F. Nori, Phys. Rev. A **99**, 012302 (2019).
[10] P. Kómár, E. M. Kessler, M. Bishof, L. Jiang, A. S. Sørensen, J. Ye, and M. D. Lukin, Nat. Phys. **10**, 582 (2014).
[11] T. J. Proctor, P. A. Knott, and J. A. Dunningham, Phys. Rev. Lett. **120**, 080501 (2018).
[12] R. Raussendorf and H. J. Briegel, Phys. Rev. Lett. **86**, 5188 (2001).
[13] P. Walther, K. J. Resch, T. Rudolph, E. Schenck, H. Weinfurter, V. Vedral, M. Aspelmeyer, and A. Zeilinger, Nature **434**, 169 (2005).
[14] A. Broadbent, J. Fitzsimons, and E. Kashefi, in *Proceedings of the 2009 50th Annual IEEE Symposium on Foundations of Computer Science*, FOCS '09 (IEEE Computer Society, Washington, DC, USA, 2009) pp. 517–526.
[15] S. Barz, E. Kashefi, A. Broadbent, J. F. Fitzsimons, A. Zeilinger, and P. Walther, Science **335**, 303 (2012).
[16] K. Chen and H.-K. Lo, Quantum Info. Comput. **7**, 689 (2007).
[17] H.-K. Lo, M. Curty, and K. Tamaki, Nat. Photon. **8**, 595 EP (2014).
[18] M. Epping, H. Kampermann, C. macchiavello, and D. Bruß, New J. Phys. **19**, 093012 (2017).
[19] M. Hein, J. Eisert, and H. J. Briegel, Phys. Rev. A **69**, 062311 (2004).
[20] T. E. Northup and R. Blatt, Nat. Photon. **8**, 356 EP (2014).
[21] C. Monroe, R. Raussendorf, A. Ruthven, K. R. Brown, P. Maunz, L.-M. Duan, and J. Kim, Phys. Rev. A **89**, 022317 (2014).
[22] A. Reiserer and G. Rempe, Rev. Mod. Phys. **87**, 1379 (2015).
[23] A. Sipahigil, R. E. Evans, D. D. Sukachev, M. J. Burek, J. Borregaard, M. K. Bhaskar, C. T. Nguyen, J. L. Pacheco, H. A. Atikian, C. Meuwly, R. M. Camacho, F. Jelezko, E. Bielejec, H. Park, M. Lončar, and M. D. Lukin, Science **354**, 847 (2016).
[24] N. Kalb, A. A. Reiserer, P. C. Humphreys, J. J. W. Bakermans, S. J. Kamerling, N. H. Nickerson, S. C. Benjamin, D. J. Twitchen, M. Markham, and R. Hanson, Science **356**, 928 (2017).
[25] A. Pirker, J. Wallnöfer, and W. Dür, New J. Phys. **20**, 053054 (2018).
[26] P. C. Humphreys, N. Kalb, J. P. J. Morits, R. N. Schouten, R. F. L. Vermeulen, D. J. Twitchen, M. Markham, and R. Hanson, Nature **558**, 268 (2018).
[27] K. S. Chou, J. Z. Blumoff, C. S. Wang, P. C. Reinhold, C. J. Axline, Y. Y. Gao, L. Frunzio, M. H. Devoret, L. Jiang, and R. J. Schoelkopf, Nature **561**, 368 (2018).
[28] B. Jing, X.-J. Wang, Y. Yu, P.-F. Sun, Y. Jiang, S.-J. Yang, W.-H. Jiang, X.-Y. Luo, J. Zhang, X. Jiang, X.-H. Bao, and J.-W. Pan, Nat. Photon. **13**, 210 (2019).
[29] Y. Yu, F. Ma, X.-Y. Luo, B. Jing, P.-F. Sun, R.-Z. Fang, C.-W. Yang, H. Liu, M.-Y. Zheng, X.-P. Xie, W.-J. Zhang, L.-X. You, Z. Wang, T.-Y. Chen, Q. Zhang, X.-H. Bao, and J.-W. Pan, Nature **578**, 240 (2020).
[30] R. Horodecki, P. Horodecki, M. Horodecki, and K. Horodecki, Rev. Mod. Phys. **81**, 865 (2009).
[31] O. Gühne and G. Tóth, Phys. Rep. **474**, 1 (2009).
[32] W. McCutcheon, A. Pappa, B. A. Bell, A. McMillan, A. Chailloux, T. Lawson, M. Mafu, D. Markham, E. Diamanti, I. Kerenidis, J. G. Rarity, and M. S. Tame, Nat. Commun. **7**, 13251 (2016).
[33] H. M. Wiseman, S. J. Jones, and A. C. Doherty, Phys. Rev. Lett. **98**, 140402 (2007).
[34] S. J. Jones, H. M. Wiseman, and A. C. Doherty, Phys. Rev. A **76**, 052116 (2007).

[35] C.-M. Li, K. Chen, Y.-N. Chen, Q. Zhang, Y.-A. Chen, and J.-W. Pan, Phys. Rev. Lett. **115**, 010402 (2015).

[36] A. Pappa, A. Chailloux, S. Wehner, E. Diamanti, and I. Kerenidis, Phys. Rev. Lett. **108**, 260502 (2012).

[37] See Supplementary Material for definition of graph states, definition and discussion of classical nodes, detailed deriviation of the fidelity function, discussion on genuine multi-subsystem EPR steering, and details of optimal cheating strategy (OSC) and its experimental results.

[38] M. A. Nielsen and I. L. Chuang, *Quantum Computation and Quantum Information* (Cambridge University Press, 2010).

[39] D. F. V. James, P. G. Kwiat, W. J. Munro, and A. G. White, Phys. Rev. A **64**, 052312 (2001).

[40] N. D. Mermin, Rev. Mod. Phys. **65**, 803 (1993).

[41] O. Gühne, G. Tóth, P. Hyllus, and H. J. Briegel, Phys. Rev. Lett. **95**, 120405 (2005).

[42] N. Brunner, D. Cavalcanti, S. Pironio, V. Scarani, and S. Wehner, Rev. Mod. Phys. **86**, 419 (2014).

[43] C.-M. Li, K. Chen, A. Reingruber, Y.-N. Chen, and J.-W. Pan, Phys. Rev. Lett. **105**, 210504 (2010).

[44] N. D. Mermin, Phys. Rev. Lett. **65**, 3373 (1990).

[45] A. Peres, Phys. Lett. A **151**, 107 (1990).

[46] A. Cabello, Phys. Rev. Lett. **101**, 210401 (2008).

[47] E. Amselem, M. Rådmark, M. Bourennane, and A. Cabello, Phys. Rev. Lett. **103**, 160405 (2009).

[48] G. Kirchmair, F. Zähringer, R. Gerritsma, M. Kleinmann, O. Gühne, A. Cabello, R. Blatt, and C. F. Roos, Nature **460**, 494 (2009).

[49] Q. Y. He and M. D. Reid, Phys. Rev. Lett. **111**, 250403 (2013).

[50] A. J. Bennet, D. A. Evans, D. J. Saunders, C. Branciard, E. G. Cavalcanti, H. M. Wiseman, and G. J. Pryde, Phys. Rev. X **2**, 031003 (2012).

[51] T. Monz, P. Schindler, J. T. Barreiro, M. Chwalla, D. Nigg, W. A. Coish, M. Harlander, W. Hänsel, M. Hennrich, and R. Blatt, Phys. Rev. Lett. **106**, 130506 (2011).

[52] G. H. Aguilar, T. Kolb, D. Cavalcanti, L. Aolita, R. Chaves, S. P. Walborn, and P. H. Souto Ribeiro, Phys. Rev. Lett. **112**, 160501 (2014).

[53] L. Aolita, F. de Melo, and L. Davidovich, Rep. Prog. Phys. **78**, 042001 (2015).

[54] M. Walter, B. Doran, D. Gross, and M. Christandl, Science **340**, 1205 (2013).

[55] Y.-H. Kim, S. P. Kulik, M. V. Chekhova, W. P. Grice, and Y. Shih, Phys. Rev. A **67**, 010301 (2003).

[56] X.-C. Yao, T.-X. Wang, P. Xu, H. Lu, G.-S. Pan, X.-H. Bao, C.-Z. Peng, C.-Y. Lu, Y.-A. Chen, and J.-W. Pan, Nature Photonics **6**, 225 EP (2012).

[57] B. Jungnitsch, S. Niekamp, M. Kleinmann, O. Gühne, H. Lu, W.-B. Gao, Y.-A. Chen, Z.-B. Chen, and J.-W. Pan, Phys. Rev. Lett. **104**, 210401 (2010).

SUPPLEMENTARY INFORMATION

GRAPH STATES

Suppose that each quantum node is a quantum two-dimensional system (qubit). An edge, say $(i,j) \in E$, corresponds to a two-qubit conditional transformation among the two qubits (vertices) i and j by $U_{(i,j)} = \sum_{v_i=0}^{1} |v_i\rangle\langle v_i| \otimes (Z_j)^{v_i}$, where $\{|v_i\rangle\}$ is an orthonormal basis of the ith qubit and $Z_j = \sum_{v_j=0}^{1} (-1)^{v_j} |v_j\rangle\langle v_j|$. The state vector of a graph state is determined by the target graph $G(V,E)$, where $|V| = N$ indicates the total node number and E tells us how the nodes are connected together to show the network topology; that is,

$$|G\rangle = \prod_{(i,j)\in E} U_{(i,j)} |f_0\rangle, \qquad (7)$$

where $|f_0\rangle = [(|0\rangle + |1\rangle)/\sqrt{2}]^{\otimes N}$ is the initial state of the network.

FIDELITY FUNCTION $F(N)$

For a N-node network in arbitrary graph state $|G\rangle$ as shown in the main text, the value of the fidelity function $F(N)$ under given experimental results shows the fidelity of the created network and the target graph state. The way the graph state $|G\rangle\langle G|$ is decomposed decides the construction of the fidelity function, which can be understood by the following explicit general decomposition for arbitrary graph states [38, 39]

$$|G\rangle\langle G| = \sum_{\vec{m}} h_{\vec{m}} \bigotimes_{k=1}^{N} \hat{R}_{m_k}, \qquad (8)$$

where $\hat{R}_{m_k}$ represents the m_kth observable of the kth qubit. For instance, suppose that the created network is in a N-qubit state described by a density operator ρ_{expt}, the network fidelity function of ρ_{expt} and $|G\rangle\langle G|$ satisfies the relation

$$F(N) = \text{tr}(\rho_{\text{expt}} |G\rangle\langle G|)$$
$$= \sum_{\vec{m}} h_{\vec{m}} \langle R_{m_1}...R_{m_N}\rangle, \qquad (9)$$

where $\langle R_{m_1}...R_{m_N}\rangle = \text{tr}(\rho_{\text{expt}} \bigotimes_{k=1}^{N} \hat{R}_{m_k})$.

In this work, we assume that the measurements on each qubit are performed with the observables in the Pauli matrices, $\{\hat{R}_{m_k}|m_k = 0,1,2,3\}$, where $\hat{R}_0 = I$, $\hat{R}_1 = X$, $\hat{R}_2 = Y$, and $\hat{R}_3 = Z$. The spectral decomposition of the Pauli matrices: $\hat{R}_0 = \sum_{v_{m_k}=\pm1} |v_{m_k}\rangle_{m_k m_k}\langle v_{m_k}|$, and $\hat{R}_{m_k} = \sum_{v_{m_k}=\pm1} v_{m_k} |v_{m_k}\rangle_{m_k m_k}\langle v_{m_k}|$ for $m_k = 1,2,3$, reminds us the relation between the measurement outcomes $R_0 = \text{tr}(|v_{m_k}\rangle_{m_k m_k}\langle v_{m_k}| \hat{R}_0) = 1$ and

$R_{m_k} = \text{tr}(|v_{m_k}\rangle_{m_k m_k}\langle v_{m_k}| \hat{R}_{m_k}) = v_{m_k}$ and the state of the measured qubit $|v_{m_k}\rangle_{m_k}$. Note that there are the following relationships between the different eigenstates of $\hat{R}_{m_k}$: $|\pm1\rangle_1 = (|0\rangle \pm |1\rangle)/\sqrt{2}$ and $|\pm1\rangle_2 = (|0\rangle \pm i|1\rangle)/\sqrt{2}$, where $|0\rangle \equiv |1\rangle_3$ and $|1\rangle \equiv |-1\rangle_3$ are also used in the definition of graph state (7). Therefore the states $|G\rangle\langle G|$ can be specified by the decomposition (8) using the orthonormal set of matrices, $\{\bigotimes_{k=1}^{N} \hat{R}_{m_k}/\sqrt{2}\}$, from which the fidelity function $\mathcal{F}$ is then constructed. In this case the constituent 2^N matrices with $h_{\vec{m}} = 2^{-N}$ consist of the stabilizer of the graph state [19]. In addition to Pauli matrices used here, the fidelity function can also be constructed in the same manner when the observables for state decomposition are not orthonormal.

CLASSICAL NODES

Suppose a given N-node network with the desired target graph state decays into a hybrid of quantum and classical nodes. As shown in the main text, the index set of the network nodes, V, can then be divided into the quantum-node subset, V_Q, and the classical-node subset, V_c, accordingly. We assume that there are n_c classical nodes in the hybrid network, i.e., $|V_c| = n_c$, and $|V_c| + |V_Q| = N$. Classical nodes possess physical properties that exist independent of observation [41]. The state of each classical node can be specified by a pre-existing and fixed set of measurement outcomes [33, 34]

$$\mathbf{v}_k \equiv \{R_{m_k} = v_{m_k}|m_k = 1,2,3\}, \qquad (10)$$

where $k \in V_c$. For $v_{m_k} = \pm1$, we have 8 possible such sets denoted by $\mathbf{v}_{k,\eta} = \{v_1, v_2, v_3\}$, where

$$\mathbf{v}_{k,1} = \{+1,+1,+1\}, \mathbf{v}_{k,2} = \{+1,+1,-1\},$$
$$\mathbf{v}_{k,3} = \{+1,-1,+1\}, \mathbf{v}_{k,4} = \{+1,-1,-1\},$$
$$\mathbf{v}_{k,5} = \{-1,+1,+1\}, \mathbf{v}_{k,6} = \{-1,+1,-1\},$$
$$\mathbf{v}_{k,7} = \{-1,-1,+1\}, \mathbf{v}_{k,8} = \{-1,-1,-1\}.$$

Incoherent manipulations of qubits cause the qubits to decay such that the qubit states can eventually be described by the classical realistic theory, such as measurements on qubits, and qubit storage or transmission under the action of a noisy channel.

For example, suppose that the observable Z is chosen for a measurement on the superposition state $|1\rangle_1 = (|1\rangle_3 + |-1\rangle_3)/\sqrt{2}$. After measurement, the qubit becomes a definite state in one of the two post-measurement states $|1\rangle_3$ and $|-1\rangle_3$, independent of the observation with respect to the measurement of the observable Z. That is, in terms of the classical realistic theory, if the measurement outcome is $v_3 = 1$ ($v_3 = -1$), the probability of constantly observing $v_3 = 1$ ($v_3 = -1$) under the measurement of Z is $p(v_3 = 1) = \sum_{\eta=1,3,5,7} p(\mathbf{v}_{k,\eta}) = 1$

$(p(v_3 = -1) = \sum_{\eta=2,4,6,8} p(\mathbf{v}_{k,\eta}) = 1)$, where $p(\mathbf{v}_{k,\eta})$ is the probability of being in the pre-existing state $\mathbf{v}_{k,\eta}$.

Moreover, after many rounds of the same measurements on the same initial superposition state, and taking all post-measurment states into account, the average post-measurement state, $\rho_{\text{avg}} = (|1\rangle_{33}\langle 1| + |-1\rangle_{33}\langle -1|)/2$, can be described in the same manner. One can think of ρ_{avg} as one composed of pre-existing states $\mathbf{v}_{k,\eta}$ with a probability distribution $p(\mathbf{v}_{k,\eta})$ such that $p(v_3 = 1) = \sum_{\eta=1,3,5,7} p(\mathbf{v}_{k,\eta}) = 1/2$ and $p(v_3 = -1) = \sum_{\eta=2,4,6,8} p(\mathbf{v}_{k,\eta}) = 1/2$.

From the viewpoint of physically motivated operational meaning, once we have the pre-existing recipe of $\mathbf{v}_{k,\eta}$ with the probability distribution $p(\mathbf{v}_{k,\eta})$, the post-measurement state ρ_{avg} can be prepared accordingly by incoherently mixing the states $|1\rangle_3$ and $|-1\rangle_3$. It is clear that $\mathbf{v}_{k,\eta}$ exist independent of observation; after all, the prescribed information about $\mathbf{v}_{k,\eta}$ has been shown in the pre-existing recipe.

The descriptions of the classical nodes illustrated above can be directly applied to the cases where qubit storage or transmission undergoes noisy channels, such as the final state $|v_3\rangle_3$ which results from the initial state $|1\rangle_1$ through an amplitude damping channel, and the complete mixed state ρ_{avg} derived from $|1\rangle_1$ via a full decoherence process.

SET OF GRADUATIONS $\{\mathcal{F}_{n_c}\}$

To examine the minimum deviation of a N-node network with n_c classical nodes from the target graph state, we evaluate the maximum fidelity by performing the following task

$$\mathcal{F}_{n_c} = \max_{V_c, \{R_{m_k}\}} F, \qquad (11)$$

where the maximization is over all vertex sets V_c with $|V_c| = n_c$ and all outcomes from measurements on the classical and quantum nodes, $\{R_{m_k}\}$. Next, we illustrate the step-by-step derivation for Eq. (3-6) in the main text. The fidelity (11) is determined in three steps:

First, as shown in Eq. (3) in the main text, before the state decay, when explicitly considering Eq. (11), the state vector of the target graph state can always be represented in the Schmidt form of rank r [43]

$$|G\rangle = \frac{1}{\sqrt{r}} \sum_{v=0}^{r-1} |v\rangle_{sQ} |v\rangle_{sc}, \qquad (12)$$

for $r \geq 2$, where $\{|v\rangle_{sQ}\}$ and $\{|v\rangle_{sc}\}$ are the Schmidt bases for the nodes in the vertex sets V_Q and V_c, respectively. This representation shows us the following form under the state decomposition for the nodes in V_c

$$|G\rangle\langle G| = \frac{1}{r} \sum_{v,v',\vec{m}_c} h_{\vec{m}_c}^{vv'} |v\rangle_{sQsQ}\langle v'| \bigotimes_{k\in V_c} \hat{R}_{m_k}, \qquad (13)$$

where $|v\rangle_{scsc}\langle v'| = \sum_{\vec{m}_c} h_{\vec{m}_c}^{vv'} \bigotimes_{k\in V_c} \hat{R}_{m_k}$, $\vec{m}_c \equiv \{m_k | k \in V_c\}$, and $h_{\vec{m}_c}^{vv'}$ denote the decomposition coefficients. Alternatively, it can be represented in the matrix form in the basis, $\{|v\rangle_{sQ}\}$. Let us take $r = 2$ for example, we have

$$|G\rangle\langle G| = \begin{pmatrix} \hat{f}_{00} & \hat{f}_{01} \\ \hat{f}_{10} & \hat{f}_{11} \end{pmatrix}, \qquad (14)$$

where $\hat{f}_{vv'} = 1/2 \sum_{\vec{m}_c} h_{\vec{m}_c}^{vv'} \bigotimes_{k\in V_c} \hat{R}_{m_k}$.

Second, we use the classical realistic theory to give a complete description of the total state of the n_c classical nodes in terms of the pre-existing outcome sets: $\{\mathbf{v}_k | k \in V_c\}$. The network fidelity function (Function) can be rephrased as the following explicit form

$$F = \frac{1}{r} \sum_{v,v',\vec{m}_c} h_{\vec{m}_c}^{vv'} \left\langle |v\rangle_{sQsQ}\langle v'| \right\rangle \left\langle \prod_{k\in V_c} R_{m_k} \right\rangle. \qquad (15)$$

Note that R_{m_k} are the pre-existing outcomes given in $\mathbf{v}_k$ (10) where $\mathbf{v}_k \in \{\mathbf{v}_{k,\eta} | \eta = 1, 2, ..., 8\}$.

Finally, through the expression (15) for the fidelity function, the maximization task (11) becomes

$$\mathcal{F}_{n_c} = \max_{\{\mathbf{v}_k | k \in V_c\}} E\left[\begin{pmatrix} f_{00} & f_{01} \\ f_{10} & f_{11} \end{pmatrix}\right], \qquad (16)$$

where $f_{vv'} = 1/2 \sum_{\vec{m}_c} h_{\vec{m}_c}^{vv'} \langle \prod_{k\in V_c} R_{m_k} \rangle$ and $E[\cdot]$ denotes the largest eigenvalue of the matrix represented in the orthonormal basis $\{|0\rangle_{sQ}, |1\rangle_{sQ}\}$. Note that, given a set of $f_{vv'}$, the eigenvector of $E[\cdot]$ correspond to the state of quantum nodes. Here $r = 2$ is shown to be necessary for the maximum of F. One always can find at least one bipartite splitting of the network nodes in the target graph to have such Schmidt rank of state decomposition under the condition $|V_c| = n_c$. When the fidelity functions are specified in the orthonormal sets of Pauli matrices and the classical nodes are described under the assumption of realism [41] given in (10), we obtain

$$f_{00} = \frac{1}{2}, f_{01} = \frac{1}{2^{n_c+1}}(1+i)^{n_c},$$
$$f_{10} = \frac{1}{2^{n_c+1}}(1-i)^{n_c}, f_{11} = 0. \qquad (17)$$

Thus we arrive the result of Eq. (6) in the main text by calculating the maximum eigenvalue of the matrix with the above matrix elements. From the viewpoint of the operational meaning, as the quantum nodes are prepared in the eigenstate of such maximum eigenvalue and the classical nodes are in a specific state $\{\mathbf{v}_k | k \in V_c\}$, the resulting hybrid of quantum and classical nodes can show the best fidelity, $\mathcal{F}_{n_c}$.

It is worth noting that the choice of $\{\mathbf{v}_k | k \in V_c\}$ for the maximum eigenvalue $\mathcal{F}_{n_c}$ is not unique. Then there exist alternative to the matrix elements $f_{vv'}$ (17) for matrices with the same maximum eigenvalue, $\mathcal{F}_{n_c}$, but different

eigenvectors. This also means that there are more than one quantum-classical hybrids that can be used to achieve the best fidelity, $\mathcal{F}_{n_c}$.

Next, we give a concrete example of three-qubit star-graph (or chain-graph) state to illustrate the three steps in our method for determining $\mathcal{F}_{n_c}$ (11). According to (7) and (12) a three-qubit star-graph state can be expressed as

$$\left| G_3^{star} \right\rangle = \frac{1}{\sqrt{2}} (|0\rangle_{sQ} |0\rangle_{sc} + |1\rangle_{sQ} |1\rangle_{sc}).$$

As will be shown bellow, the Schmidt basis $\{|0\rangle_{sc}, |1\rangle_{sc}\}$ corresponds to either one ($n_c = 1$) or two ($n_c = 2$) nodes in V_c.

In the case of $n_c = 1$, we assume that the 3rd qubit is the node belonging to V_c and connected with the other two qubits in V_Q. Then we have

$$\{|0\rangle_{sQ} = |1\rangle_1 |1\rangle_1, |1\rangle_{sQ} = |-1\rangle_1 |-1\rangle_1\},$$

and

$$\{|0\rangle_{sc} = |1\rangle_3, |1\rangle_{sc} = |-1\rangle_3\}.$$

With the following explicit decomposition for the nodes in V_c:

$$|0\rangle_{scsc}\langle 0| = \frac{1}{2}(\hat{R}_0 + \hat{R}_3), |0\rangle_{scsc}\langle 1| = \frac{1}{2}(\hat{R}_1 + i\hat{R}_2),$$
$$|1\rangle_{scsc}\langle 0| = \frac{1}{2}(\hat{R}_1 - i\hat{R}_2), |1\rangle_{scsc}\langle 1| = \frac{1}{2}(\hat{R}_0 - \hat{R}_3),$$

we obtain Eq. (13). As the 3rd qubit decays to a classical node which can be specified by a pre-existing state $\mathbf{v}_3$, any observable in the classical node has a predetermined value that exists independent of observation according to (10), and from which we arrive at Eq. (15). When setting $\mathbf{v}_3$ as $\mathbf{v}_{3,1}$, we obtain the results of Eq. (17) with

$$f_{00} = \frac{1}{2}, f_{01} = \frac{1}{4}(1 + i), f_{10} = \frac{1}{4}(1 - i), f_{11} = 0,$$

and the minimum deviation of a network mixed with a single classical node:

$$\mathcal{F}_1 \simeq 0.6830,$$

as shown in Eq. (2) for $n_c = 1$ in the main text.

Similarly, in the case of $n_c = 2$, where the 3rd qubit is assumed to be in V_Q and connected with the other two qubits in V_c, we have

$$\{|0\rangle_{sQ} = |1\rangle_3, |1\rangle_{sQ} = |-1\rangle_3\},$$

and

$$\{|0\rangle_{sc} = |1\rangle_1 |1\rangle_1, |1\rangle_{sc} = |-1\rangle_1 |-1\rangle_1\}.$$

To derive Eq. (13), the following state decomposition is used

$$|0\rangle_{scsc}\langle 0| = \frac{1}{4}(\hat{R}_0\hat{R}_0 + \hat{R}_0\hat{R}_1 + \hat{R}_1\hat{R}_0 + \hat{R}_1\hat{R}_1),$$

$$|0\rangle_{scsc}\langle 1| = \frac{1}{4}(-\hat{R}_2\hat{R}_2 - i\hat{R}_2\hat{R}_3 - i\hat{R}_3\hat{R}_2 + \hat{R}_3\hat{R}_3),$$

$$|1\rangle_{scsc}\langle 0| = \frac{1}{4}(-\hat{R}_2\hat{R}_2 + i\hat{R}_2\hat{R}_3 + i\hat{R}_3\hat{R}_2 + \hat{R}_3\hat{R}_3),$$

$$|1\rangle_{scsc}\langle 1| = \frac{1}{4}(\hat{R}_0\hat{R}_0 - \hat{R}_0\hat{R}_1 - \hat{R}_1\hat{R}_0 + \hat{R}_1\hat{R}_1).$$

When the 1st and the 2nd qubits decay into two classical nodes which can be specified by the pre-existing states of $\mathbf{v}_1$ and $\mathbf{v}_2$, respectively, the fidelity function (9) becomes Eq. (15), and any observable in the two classical nodes has a predetermined value that exists independent of observation according to (10). As $\mathbf{v}_1 = \mathbf{v}_{1,3}$ and $\mathbf{v}_2 = \mathbf{v}_{2,3}$, we obtain the elements of the matrix represented in the orthonormal basis [see Eqs. (16) and (17)]:

$$f_{00} = \frac{1}{2}, f_{01} = \frac{i}{4}, f_{10} = -\frac{i}{4}, f_{11} = 0,$$

and from which we get the the maximum fidelity for a network consisting of one quantum node and two classical nodes:

$$\mathcal{F}_2 \simeq 0.6036.$$

This result consistent with Eq. (2) for $n_c = 2$ shown in the main text.

GENUINE MULTI-SUBSYSTEM EPR STEERING

Satisfying the criterion

$$F > \mathcal{F}_{n_c}, \tag{18}$$

confirms that, the correlation between the network nodes of a created state is stronger than all the correlations that can be created by the quantum-node subsets, V_Q, and the classical-node subsets, V_c with $|V_c| = n_c$, for all possible bipartitions of the hybrid of quantum and classical nodes. This concretely describes the steering effects between two subsystems with n_c and n_q nodes, respectively. Moreover, since all possible configurations of splitting N nodes into two subsystems are considered in the criterion, we call such steerability the genuine multi-subsystem EPR steering. This description generalizes the concept of genuine multipartite EPR steering [35, 49], where only the extreme value of $\mathcal{F}_{n_c}$ is involved. Such steerability is shown if the created network with a fidelity that goes beyond the threshold

$$\max_{n_c, V_c, \{R_{m_k}\}} F = \max_{n_c} \mathcal{F}_{n_c}. \tag{19}$$

From the result of $\mathcal{F}_{n_c}$, it is clear that $\mathcal{F} > \mathcal{F}_1$ is a fidelity criterion for genuine multipartite EPR steering.
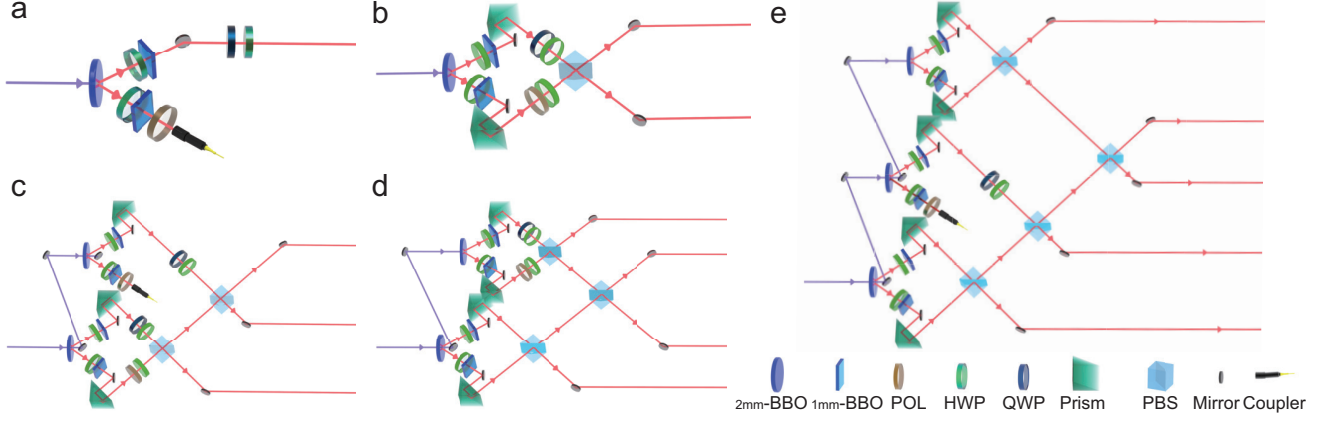
FIG. 4. Experimental setups for realizing quantum networks with $n_q + n_c$ nodes. (a-e) setup to implement networks of $n_q = 1$, $n_q = 2$, $n_q = 3$, $n_q = 4$ and $n_q = 5$, respectively.
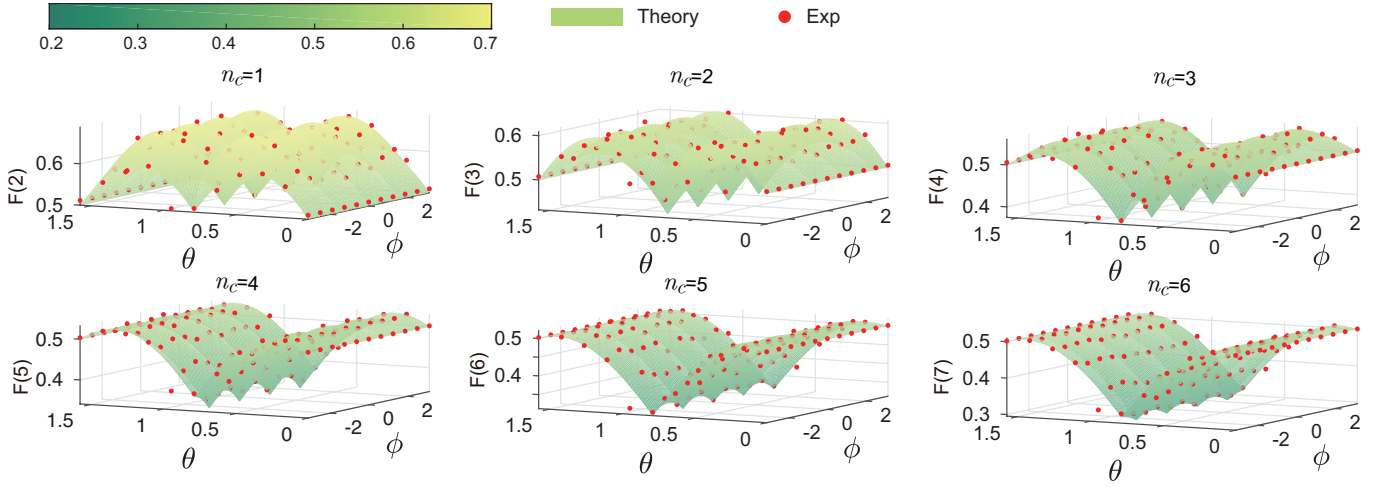

FIG. 5. Experimental results of network fidelity in the case of $n_q = 1$ with different θ and ϕ setting. The landscapes are theoretical results. The experimental results are show with red dots. The errors are shown with red bars, which are too small to recognize in the presented scale. (a)∼(f) show the cases of $n_c = 1$ to $n_c = 6$, respectively.

OPTIMAL CHEATING STRATEGY (OCS) AND ITS EXPERIMENTAL REALIZATION

In the N-node network with n_c untrusted (classical) nodes and n_q trusted (quantum) nodes, the n_c untrusted nodes prepare the entangled state $|\xi\rangle_{n_q}$ based on their knowledge of the network fidelity function $F(N)$. Combining with the measurement results of prepared $|\xi\rangle_{n_q}$, the n_c untrusted nodes broadcast their results $\in \{+1, -1\}$, according to the measurement setting for the network fidelity function. In this section, we detail the experimental state preparation of quantum networks with $N = n_c + n_q$ nodes.

$n_c = 0$

As we mentioned in the main text, we test our procedure on multiphoton graph state in star graph, which is equivalent to N-photon Greenberger-Horne-Zeilinger (GHZ) state via local operation and classical communication (LOCC). The building block to generate a N-photon GHZ state is entangled photon pair from spontaneous parametric down conversion (SPDC). Experimentally, we use an ultraviolet pulse (with central wavelength of 390nm, pulse duration of 140fs) to pump a 2mm Beta Barium Borate (BBO) crystal (as shown in Fig. 4a). The generated twin photons are entangled both in polarization degree of freedom (DOF) and frequency DOF, and separated with opening angle of 6°. To compensate the time and spatial walk-off, an half-wave plate set at 45° and a 1mm BBO crystal are inserted in each path. Using narrow-band filters with full-width at half maximum

(λ_{FWHM}) of 3 nm, the maximally entangled photon pair can be obtained $|GHZ\rangle_2 = \frac{1}{\sqrt{2}}(|HH\rangle + |VV\rangle)$. The generated photons are highly frequency-correlated, which is not suitable for multiphoton experiments. To enhance the multiphoton coincidence count rate, we recombine the generated photons on a polarization beam splitter (PBS) to eliminate frequency correlation[55, 56] (similar to the setup shown in Fig. 4b, but remove polarizer (POL), quarter-wave plate (QWP) and one HWP). By properly choosing narrow bandpass filters (full-width half-maximum (FWHM) of 3nm and 8nm in our experiment), we can obtain $|GHZ\rangle_2$ with higher counter rate.

To generate $|GHZ\rangle_3$, the ultraviolet pulse goes to shine another 2mm BBO crystal. A heralded single-photon source is obtained by triggering one photon of the second entangled photon pair. The heralded single-photon is rotated to $|+\rangle = \frac{1}{\sqrt{2}}(|H\rangle + |V\rangle)$ and then superposed with one photon from the first $|GHZ\rangle_2$ on a PBS. When two photons arrive at PBS simultaneously and come out from two output ports, $|GHZ\rangle_3$ can be obtained. The setup is shown in Fig. 4c.

$|GHZ\rangle_4$ is generated without triggering one photon from the second SPDC (as shown in Fig. 4d). Similarly, by successively shinning a third BBO crystal and proper operations, $|GHZ\rangle_5$ and $|GHZ\rangle_6$ can be obtained (as shown in Fig. 4e and Fig. 1b in the main text).

$$n_c = 1$$

To show the optimal "cheating strategy" (OCS) for quantum network $|GHZ\rangle_N$ with $n_c = 1$, first, we have the following state decomposition according to Eq. (13):

$$|GHZ\rangle_{NN}\langle GHZ| = \frac{1}{2}\sum_{k,l=H,V} |k\rangle^{\otimes N-1 \otimes N-1}\langle l| \otimes |k\rangle\langle l|.$$

(20)

Alternatively, the above state decomposition can be represented in the matrix form in the basis $\{|H\rangle^{\otimes N-1}, |V\rangle^{\otimes N-1}\}$ of the qubits in V_Q:

$$|GHZ\rangle_{NN}\langle GHZ| = \frac{1}{2}\begin{pmatrix} |H\rangle\langle H| & |H\rangle\langle V| \\ |V\rangle\langle H| & |V\rangle\langle V| \end{pmatrix}$$
$$= \frac{1}{2}\begin{pmatrix} \frac{1}{2}(I+Z) & \frac{1}{2}(X+iY) \\ \frac{1}{2}(X-iY) & \frac{1}{2}(I-Z) \end{pmatrix},$$

where $Z \equiv |H\rangle\langle H| - |V\rangle\langle V|$, $X \equiv |H\rangle\langle V| + |V\rangle\langle H|$, and $Y \equiv -i|H\rangle\langle V| + i|V\rangle\langle H|$ for the qubit in V_Q. Note that the last matrix form corresponds to Eq. (14).

Secondly, suppose that $|H\rangle \equiv |1\rangle_3$ and $|V\rangle \equiv |-1\rangle_3$ and apply the assumption of classical state $\mathbf{v}_{k,1} = \{+1, +1, +1\}$ to the node in V_c, the above matrix becomes

$$\begin{pmatrix} \frac{1}{2} & \frac{1}{4}(1+i) \\ \frac{1}{4}(1-i) & 0 \end{pmatrix},$$

(21)

where the matrix elements are consistent with the ones shown in Eq. (17) for $n_c = 1$. Then, the maximum eigenvalue of this matrix is just the threshold fidelity, $\mathcal{F}_1 \simeq 0.6830$; the corresponding eigenvector is $|\xi\rangle_{N-1} = \cos\theta |H\rangle^{\otimes N-1} + \sin\theta e^{i\phi}|V\rangle^{\otimes N-1}$ of the quantum nodes, where $\sin\theta = \frac{1}{\sqrt{3+\sqrt{3}}}$ and $\phi = -\frac{\pi}{4}$. That is, as the quantum nodes are prepared in $|\xi\rangle_{N-1}$ and the classical node is in the state $\mathbf{v}_{k,1}$, the OCS can be achieved to show the best fidelity of $|GHZ\rangle_N$ and the hybrid of quantum and classical nodes, $\mathcal{F}_1$.

Experimentally, the preparation of $|\xi\rangle_{N-1}$ can be performed by projecting $|GHZ\rangle_N$ onto the state $|\xi'\rangle = \cos\theta |H\rangle + \sin\theta e^{-i\phi}|V\rangle$ with QWP and POL shown in Fig. 1d in the main text. By properly choosing the angles of QWP and POL, projection of arbitrary $|\xi'\rangle$ can be realized. As explained in the section of classical nodes, such measurement can make a quantum node classical, which results in $n_c = 1$ required in the present cheating scenario.

In the case of $N = 6$ with $n_c = 1$ and $n_q = 5$ shown in Fig. 1 in the main text, we experimentally realize OCS by projecting one photon from $|GHZ\rangle_6$ on $|\xi'\rangle = \cos\theta |H\rangle + \sin\theta e^{-i\phi}|V\rangle$ (see Fig. 1d in the main text), which leaves five trusted nodes sharing a five-photon state $|\xi\rangle_5 = \cos\theta |H\rangle^{\otimes 5} + \sin\theta e^{i\phi}|V\rangle^{\otimes 5}$. Since the choice of $\mathbf{v}_k$ for the maximum eigenvalue $\mathcal{F}_1$ is not unique, the choice of θ and ϕ in OCS is not unique as well, so that they constitute an ensemble denoted as $\{|\xi\rangle_5\}$. In our experiment, we select $\sin\theta = \frac{1}{\sqrt{3+\sqrt{3}}}$ and $\phi = -\frac{\pi}{4}$ for $\mathbf{v}_k = \mathbf{v}_{k,1}$ as shown above. One can choose other pre-existing states to achieve OCS, such as $\mathbf{v}_k = \mathbf{v}_{k,2}$. For such an alternative, one needs to perform the projection onto the state $|\xi'\rangle$ with $\sin\theta = \frac{1}{\sqrt{3-\sqrt{3}}}$ and $\phi = -\frac{\pi}{4}$. We also experimentally reconstruct the landscape of network fidelity in the case of $n_q = 1$ with different θ and ϕ setting. The results are shown in Fig. 5

The trusted nodes use the experimental setup shown in Fig. 1c to measure the expected value of $\hat{R}_{m_k}$, in which the transmitted photons are projected on eigenstate $|+1\rangle_{m_k}$ of $\hat{R}_{m_k}$ with eigenvalue $+1$, while the reflected photons are projected on $|-1\rangle_{m_k}$ of $\hat{R}_{m_k}$ with eigenvalue -1. The angle setting of QWP and HWP to perform measurements of X, Y and Z are shown in Table. I. Thus, the expected value of $\langle \hat{R}_{m_k}\rangle$ can be obtained by $\frac{N_{+1}-N_{-1}}{N_{+1}+N_{-1}}$, where $N_{+1(-1)}$ is the recorded counts on detector behind transmitted (reflected) photon. For $\hat{R}_{m_k} = I$, the angle setting of QWP and HWP can be arbitrarily chosen, and $\langle I\rangle = \frac{N_{+1}+N_{-1}}{N_{+1}+N_{-1}} = 1$. Then, combining the results from untrusted node $\in \{+1, -1\}$ according to the measurement setting for the network fidelity function (1) in the main text, we obtain the network fidelity $F(6) = 0.538 \pm 0.007$, shown with red bar in Fig. 2c in the main text. We emphasize that for the case of $n_c = 1$ and
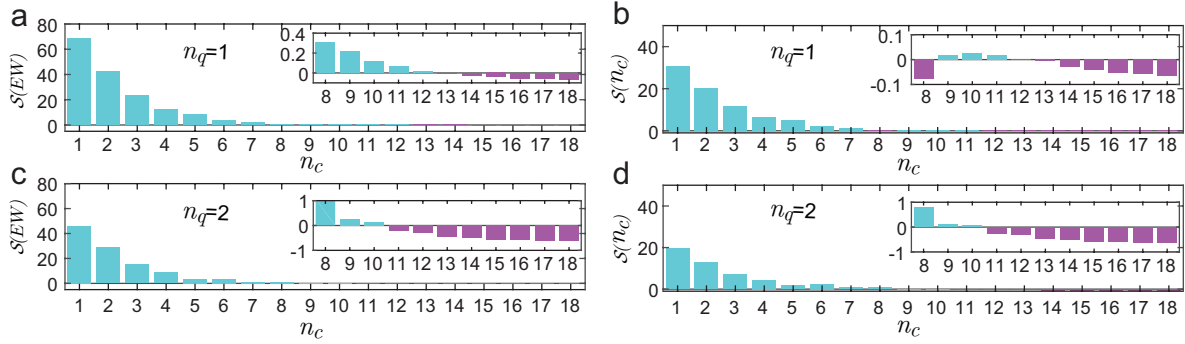
FIG. 6. Experimental results of statistical significance $\mathcal{S}(EW)$ and $\mathcal{S}(n_c)$ for witnessing entanglement and counting classical nodes, respectively. (a) $\mathcal{S}(EW)$ and (b) $\mathcal{S}(n_c)$ in quantum networks with $n_q = 1$. (c) $\mathcal{S}(EW)$ and (d) $\mathcal{S}(n_c)$ in quantum networks with $n_q = 2$. The cyan bars represent positive deviation and magenta bars represent negative deviation. The insets are $\mathcal{S}(EW)$ and $\mathcal{S}(n_c)$ from $n_c = 8$ to $n_c = 18$ in enlarged scale.

$n_q = 6$, we choose the OCS of $n_c \geq 2$, which means we experimentally prepare a six-photon state to simulate the seven-node network with one photon projected on $|\xi'\rangle$.

Observable	QWP	HWP	Expected value
X	45°	22.5°	
Y	0°	22.5°	$\frac{N_{+1}-N_{-1}}{N_{+1}+N_{-1}}$
Z	0°	0°	

TABLE I. Angle setting of QWP and HWP in X, Y, Z detection.

$$n_c \geq 2$$

For general $|GHZ\rangle_N$ with $2 \leq n_c < N$, we have the following state decomposition according to Eq. (13)

$$|GHZ\rangle_{NN}\langle GHZ| = \frac{1}{2}\begin{pmatrix} \frac{1}{2^{n_c}}(I+Z)^{\otimes n_c} & \frac{1}{2^{n_c}}(X+iY)^{\otimes n_c} \\ \frac{1}{2^{n_c}}(X-iY)^{\otimes n_c} & \frac{1}{2^{n_c}}(I-Z)^{\otimes n_c} \end{pmatrix},$$

in the basis $\{|H\rangle^{\otimes n_q}, |V\rangle^{\otimes n_q}\}$ of the qubits in V_Q. When setting $\mathbf{v}_{k,1} = \{+1, +1, +1\}$ for $k \in V_c$ under the assumption of realism, we get the matrix elements as described in Eq. (17), and they constitute a matrix with a maximum eigenvalue, $\mathcal{F}_{n_c}$, and a corresponding eigenvector, $|\xi\rangle_{n_q} = \cos\theta |H\rangle^{\otimes n_q} + \sin\theta e^{i\phi}|V\rangle^{\otimes n_q}$. Therefore, to achieve OCS for $n_c \geq 2$, one needs to prepare the state of quantum nodes in $|\xi\rangle_{n_q}$ and all the classical nodes in $\mathbf{v}_{k,1}$. This corresponds to the choice of

$$\sin\theta = \frac{1}{\sqrt{2^{n_c-1} + 2 + 2^{\frac{-n_c}{2}}\sqrt{4+2^{n_c}}}},$$

and $\phi = -\frac{n_c\pi}{4}$, for achieving $\mathcal{F}_{n_c}$ in our OCS experiments.

Experimentally, we demonstrate the OCS without manipulating $|GHZ\rangle_N$ when $n_c \geq 2$, but simulate the networks with $n_c \geq 2$ by directly creating the state $|\xi\rangle_{n_q}$

instead. Recall the general OCS for arbitrary n_c: the n_c untrusted nodes prepare the entangled state $|\xi\rangle_{n_q}$ for n_q trusted nodes based on their knowledge of the network fidelity function (1) in the main text. We prepare state $|\xi\rangle_{n_q}$ with chosen θ and ϕ. The choice of θ and ϕ is dependent on n_c, which is equivalent to the network with $n_q + n_c$ nodes.

The experimental setups to simulate networks with $n_q + n_c$ nodes are shown in Fig. 4. For network with $n_q = 1$, its equivalent quantum state is a single-photon state. As shown in Fig. 4a, triggering one photon of $|GHZ\rangle_2$ on $|H\rangle$ leaves the other photon on state $|H\rangle$. Then, by applying a QWP and HWP on it, arbitrary $|\xi\rangle_1$ can be generated.

$|\xi\rangle_2$ is generated by overlapping one photon on $|\xi\rangle_1$ and another photon on $|+\rangle$ on a PBS (shown in Fig. 4b). Similar to the generation of $|GHZ\rangle_N$, $|\xi\rangle_{n_q}$ with $n_q = 3, 4, 5$ can be generated with setups shown in Fig. 4c, d and e, respectively.

STATISTICAL SIGNIFICANCE

In the main text, we analyze the standard deviation $\mathcal{E}$ of $F(N)$ in verifying entanglement and evaluating n_c, which is also related to statistical significance $\mathcal{S}$ [57]. The significance of $F(N)$ in EW is defined as $\mathcal{S}(EW) = (F(N) - 0.5)/\mathcal{E}$, where 0.5 is the threshold of EW and $\mathcal{E}$ is the statistical error of $F(N)$ in our experiment. Similarly, the significance of $F(N)$ in evaluating n_c is defined as $\mathcal{S}(n_c) = (F(N) - \mathcal{F}_{n_c-1})/\mathcal{E}$. The larger the statistical significance is, the higher confidence interval we can obtain regarding the conclusion. The significance of $F(N)$ in networks with $n_q = 1$ and $n_q = 2$ are shown in Fig. 6a and c, the value of significance of $F(N)$ in EW is greater than 3 and with maximal value of 68.5 when $n_c \leq 6$, which represents a high confidence interval in EW. Again, it indicates EW is not confidential in identification of quantum network. With our criteria (shown in

Figs. 6b and d), $F(N)$ can be employed as an confidential indicator in evaluating n_c when $n_c \leq 6$. Although $F(N)$ could exhibit graduation when $n_c \geq 7$ (insets in Figs. 6b and d), it can not be employed as a confidential indicator to evaluating n_c as $\mathcal{S}(n_c)$ goes to subtle values.